ULTRASONIC IMAGING **28,** 83-96 (2006)

Application of Three Scattering Models to Characterization of Solid Tumors in Mice

MICHAEL L. OELZE AND WILLIAM D. O'BRIEN, JR.

Bioacoustics Research Laboratory
Department of Electrical and Computer Engineering
University of Illinois at Urbana-Champaign
405 North Mathews
Urbana, Illinois 61801
oelze@uiuc.edu

Department of Bioengineering
University of Illinois at Urbana-Champaign
1304 W. Springfield Ave.
Urbana, Illinois 61801

Two mouse models of mammary cancer (a carcinoma and sarcoma) were examined using quantitative ultrasound (QUS) and three models for ultrasound backscattering. The first model that was examined was the spherical Gaussian model (SGM). The second model was the fluid-filled sphere model (FFSM) and was hypothesized to model scattering from cell nuclei with the cell cytoplasm acting as background. The third model, called the new cell model (NCM), was constructed to model backscattering from cell nuclei and cytoskeleton. The average scatterer diameters (ASDs) were estimated from regions-of-interest (ROIs) inside the tumors using all three models and then compared. The ultrasound analysis bandwidth used in the study was 16 to 27 MHz. QUS images of the tumors utilizing the ASD estimates from the three models were constructed. The ASDs were 30.3 ± 3.06 m and 25. m with the SGM, 47.3 ± m and 47.7 ± 7.01 m with the FFSM and 41.2 ± 1.39 m and 34.4 ± 5.95 m with the NCM for the carcinoma and sarcoma, respectively. statistically significant differences between the ASD estimates from the carcinomas and sarcomas were observed using the SGM and NCM but not with the FFSM.

Key words: Backscatter; quantitative ultrasound; tissue characterization.

INTRODUCTION

Tissue characterization using ultrasound has been around for more than 20 years.[1-5] Much of the early framework for tissue characterization using ultrasound backscatter and spectral techniques was developed by Lizzi et al.[2] Techniques to normalize the backscattered measurements were developed by Sigelmann and Reid, and O'Donnell and Miller.[6, 7] Specifically, Lizzi et al. developed techniques that calibrated the measurement apparatus for the backscattered power spectrum such that the results could be system-independent. The system-independent approach was critical to comparison and implementation of processing enhancements and for the eventual application to clinical practice.

Since that time, tissue characterization using ultrasound backscatter and spectral techniques developed by Lizzi et al. have been utilized in a variety of applications.[2] More specifically, the backscatter techniques have been used to differentiate diseased versus healthy

0161-7346/06 $18.00

tissue and to detect cancer. Successful clinical applications of these quantitative ultrasound (QUS) techniques have occurred in diagnosing prostate cancer and ocular tumors.[8-17] Feleppa et al. found that the ASD in ocular tumors was a strong indicator of cancer.[13] The ASD was estimated from models of the backscattered power spectrum from the tissues. Acoustic concentration (another scatterer property estimated from the backscattered power spectrum, defined as the product of the number density of scatterers times the square of the difference between the impedance of the scatterer and background) was also integral to distinguishing diagnostically between ambiguous cases.[18] In prostate cancer detection, Feleppa et al. demonstrated that scatterer property estimates (ASD and acoustic concentration) yielded greater diagnostic accuracy and lesion localization than all other noninvasive techniques combined.[14]

Tissue characterization techniques using ultrasound backscatter have also been applied to quantify breast lesions for the diagnosis of cancer. D'Astous and Foster evaluated breast lesions using the backscatter coefficient (BSC) and their studies revealed differences between fat and infiltrating ductal cancer (IDC) near the upper limit of frequencies interrogated.[4] The BSC for parenchyma was about an order of magnitude greater than those of fat and IDC, and also exhibited higher frequency dependence. Based on the BSC, the three types of tissues were distinguishable.

In a similar study, Landini et al. quantified the backscatter from breast lesions.[19] In that study, five kinds of breast tissue (fatty, fibro-fatty, scirrhosis carcinoma, medullary carcinoma and fibrosis) were examined over the frequency range of 4 to 14 MHz. The findings from this study demonstrated that Landini et al. could estimate distinct correlation functions for the five kinds of breast tissues from the backscatter.

Based on these early successes for breast cancer diagnosis using ultrasound backscatter, breast cancer studies on animal *in vivo* were conducted.[20, 21] The studies revealed that using scatterer property estimates allowed the differentiation of benign versus malignant tumors over the frequency range from 5 to 27 MHz. However, when scatterer property estimates using a spherical Gaussian model from different kinds of malignant tumors (mouse mammary carcinoma and mouse mammary sarcoma) were examined over this frequency range, no statistically significant differences were observed. The lack of statistically significant differences was hypothesized to be due to a couple of possible sources: (1) When using a broad range of ultrasonic frequencies, the models were not sensitive to microstructural differences observed from optical examination of histological sections. (2) The models were acceptable only over a smaller frequency bandwidth. Examination of optical photomicrographs indicated that significant microstructural differences existed between the two kinds of tumors.[22] The 4T1 mouse mammary carcinoma had a uniform distribution of carcinoma cells that appeared to be monomorphic in nature with minimal extracellular matrix. The sarcoma contained cells that were relatively uniform in morphology; they were oval to polygonal in shape with large prominent nuclei. However, the sarcoma did not contain a uniform distribution of cells but cells were arranged in groups usually containing less than 20 cells per group. Groups of cells were distributed at random in an abundant extracellular matrix; thus, in many areas such groups of cells were widely separated, which resulted in identifiable structural differences when compared to the carcinoma. However, these differences were not detected through the scatterer property estimates obtained from ultrasound backscatter and the SGM over the frequency range of 5 to 27 MHz.[22] If multiple scales of scattering existed in the tissue, then the models would only be valid over a particular frequency band related to the scale of the individual scattering sources. Proper segmentation of the analysis bandwidth would then allow the models to discriminate between the two kinds of tumors based on their microstructural differences or improved models could be constructed that accounted for multiple scales of scattering.

F-tests were conducted on the backscattered power spectra from the carcinomas and sarcomas.[23] The F-tests revealed that statistically significant differences existed between the backscattered power spectra from the two tumors but only when frequencies above 16 MHz were examined. These studies suggested that to distinguish between the two kinds of tumors, higher frequencies needed to be utilized and better models developed. The present study examines two new models and compares the use of these models to the SGM. The models are used to classify the mouse mammary carcinoma and mouse mammary sarcoma over the frequency ranges of 16 to 27 MHz.

METHODOLOGY

A. Development of models

1. Spherical Gaussian model (SGM)

The SGM has been used in many studies to model the backscattered power spectra from soft tissues. The SGM has been used for many years and for many applications to obtain estimates of scatter properties.[1, 5, 16] The SGM is based on several approximations (Born, no multiple scattering, plane wave propagation) for soft tissue scattering.[24, 25] Using these approximations allows for the tissue scattering to be described by a 3-D spatial autocorrelation function of the scattering medium. If a distribution of the impedance in a scattering volume can be mapped out or approximated, then the normalized backscattered power spectrum can be calculated directly from this distribution.[26]

The properties of the SGM allowed rapid classification schemes because the SGM could be linearized in log space.[20] Gating and lateral beam pattern effects were incorporated by Lizzi et al. for the SGM yielding a theoretical power spectrum.[16]

$$W_{theor}\ f \quad \frac{185 L q^2 a_{eff}^6 n_z f^4}{1\ \ 2.66\ \ f g a_{eff}}^2 e^{\ 12.3 f^2 a_{eff}^2} \tag{1}$$

where f is the frequency (MHz), a_{eff} is the effective scatterer radius (mm), n_z is the average acoustic concentration of scatterers (mm^{-3}), L is the axial length of the range gated region (Hanning window) and q is the ratio of the aperture radius to distance from the ROI. The effective scatterer radius represents the correlation length associated with a spatial impedance profile described by a Gaussian function. Estimates of the effective scatterer radius or ASD were made according to the method of Oelze et al.[20] Estimates of ASD have been hypothesized to relate to scattering from cells in a mouse mammary carcinoma model.[21] In the present study, estimates of ASD using the SGM were compared to the actual size of cells in the tumors.

The goodness of fit of the model to the measured data was assessed by the goodness-of-fit statistic, R^2, given by

$$R^2 \quad 1.0 \quad \frac{SS_{model}}{SS_{mean}} \tag{2}$$

where SS_{model} represents the sum of squares of the data minus the model for each frequency value in the spectrum and SS_{mean} represents the sum of squares of the data minus the mean

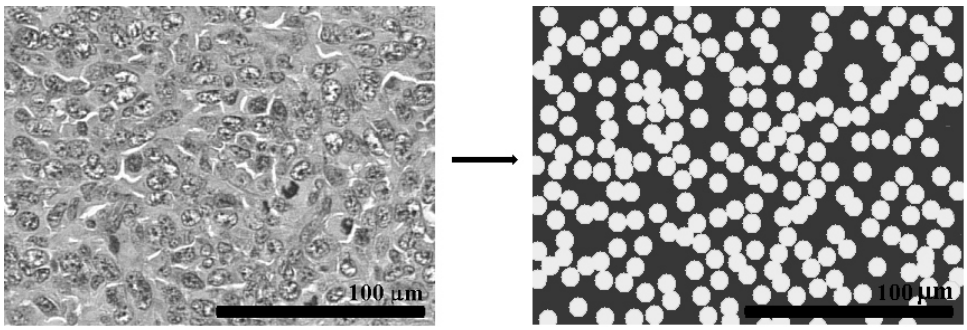

FIG. 1 Photomicrograph (left) of 4T1 mouse mammary carcinoma tumor and model of scattering from tumor (right) with nuclei as the scatterers and cytoplasm and extracellular spaces as the background.

value of the data curve for each frequency value in the spectrum (note that it is possible for the R^2 statistic to be negative). The R^2 statistic reveals how the model fits the data compared to a simple horizontal line through the mean. The closer the R^2 statistic is to 1.0 the better the fit of the model to the data. A negative value for the R^2 statistic indicates that a simple horizontal line through the mean value of the spectrum values fits data better than the model does.

2. Fluid-filled sphere model (FFSM)

Previous experiments with the carcinoma tumors and carcinoma cell pellets and comparison with the photomicrograph slides of the tumors, suggested that the cells were the dominant source of scattering.[23] Therefore, if an acoustic model of the cell could be constructed, then the frequency dependence of backscattering at higher frequencies could be better understood and predicted. Closer examination of the carcinoma tumor and cell pellets led to the initial hypothesis that the cell nucleus was the most important factor in cell scattering.[21] In the case of the carcinoma tumors and cell pellets, a model was constructed to describe the scattering based on the nucleus as a fluid-filled sphere. The cytoplasm was conjectured to serve as a background propagation medium with the nuclei representing a random distribution of scatterers. Figure 1 displays a photomicrograph of a carcinoma tumor along with a representation of the model. The nuclei, originally stained dark blue in the photomicrograph, are represented by solid circles and the cell cytoplasm and extracellular material are given a single color representing the background. As the figure suggests, the tumor is then modeled as a distribution of randomly-spaced fluid-filled spheres.

An exact solution for scattering from a fluid-filled sphere was first developed by Anderson.[27] The FFSM was used to estimate the nuclear diameter of the cells in order to parameterize the tumors. The FFSM was fit to the normalized backscattered power spectrum measured from the tumors. Four variables were used to fit the FFSM to the normalized power spectrum: (1) the ratio of compressibilities (scatterer to background), h, (2) the ratio of densities, g, (3) the nuclear diameter, D, (4) and a gain factor. The gain factor was used to correct for any magnitude bias in the normalized power spectrum measured from the tumors. The gain factor simply added or subtracted a constant from the normalized power spectrum. The ratios of compressibilities and densities were limited to the range of 0.9 to 1.1 (or 10% changes between scatterer and background). In the present study, estimates of ASD using the FFSM were compared to the actual size of the nuclei of the cells in the tumors. The goodness of fit of the model to the measured data was assessed by the goodness-of-fit statistic, R^2.

3. New cell model (NCM)

The NCM was also developed from the same hypothesis used in the FFSM that the cells were a dominant source of scattering. However, instead of assuming that the cytoplasm

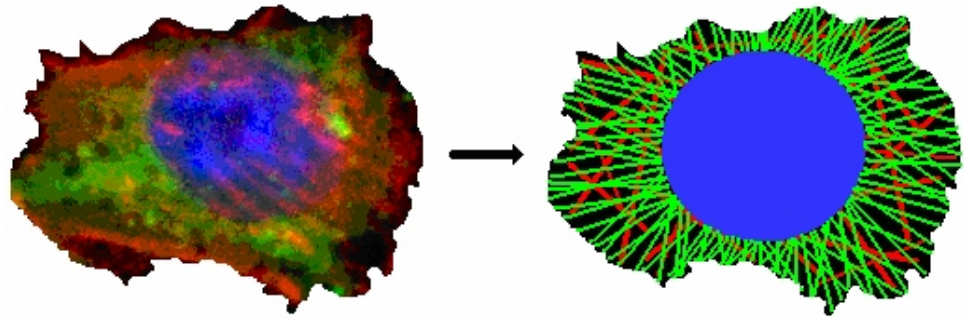

FIG. 2 Confocal microscope image (left) of 4T1 mouse mammary tumor (MMT) carcinoma cell showing the cytoskeletal elements. Actin labeled with phallicidin conjugated to Alexa 546 (red) and tubulin immunolabled with a FITC (green) conjugate. The nucleic acids were counterstained with bisbenzimide blue. Image made with Leica TCS SP2 confocal microscope (Leica Microsystems, Buffalo, NY). An idealization of the cell cytoskeletal features is displayed (right).

acted as a constant background with the nucleus as the scatterer, the cell cytoskeleton was modeled as a part of the scatterer. Figure 2a displays an image of a carcinoma cell cultured *in vitro*. The cell was adhered to a culture plate giving it the irregular shape. However, cells growing *in vivo* are less irregular and more spherical in shape. The image displays the different structural components of a cell that were used to model scattering from the cell. The actin filaments criss-cross throughout the cell body increasing the density and reducing the compressibility of the cell. Microtubules radiate from the nucleus to the edges of the cell body also increasing the density and reducing the overall compressibility of the cell. Because the microtubules radiate from the nucleus, a larger concentration of microtubules will exist near the nucleus as compared to the edge of the cell body.

A 3-D spatial autocorrelation function for the scattering medium was again used to construct the scattering model. To construct the model, a 3-D spatial mapping of the impedance was constructed and the autocorrelation function of the 3-D map was made.[25, 26] The backscattered power spectrum was then related to the 3-D spatial autocorrelation through the magnitude of the Fourier transform.

The model assumes that the scatterer (the cell) is spherically symmetric so that a mapping of its spatial impedance properties could be described by a 1-D function. Figure 3 is a graph of a hypothetical 1-D impedance function describing the cell. The 1-D impedance function in figure 3 does not necessarily represent the actual impedance value of the nucleus compared to the cytoplasm. The actual relation between the impedance of the nucleus and cell cytoplasm will be determined by fitting the backscattered power spectrum from the 1-D impedance function to the measured data. The fitting routine will determine the best estimates of I_0, I_1, R_N and R_C for which the chi-square value between the model and the measured data is minimized. The nucleus is described by a constant impedance value while the cytoskeletal features are described by a graded impedance with increasing impedance values closer to the nucleus. The model allows a discontinuity between the cell nucleus and cytoskeleton outside the nucleus. The graded impedance reflects the decreasing number density of microtubules further from the nucleus.

The model used in this study assumes that the impedance outside of the cell (extracellular matrix), I_B, is continuous at the boundary of the cell cytoskeleton (membrane) and that no discontinuity exists between the cell membrane and extracellular matrix. Examination of figure 1 reveals that the extracellular matrix is minimal in the carcinoma. Therefore, assuming the boundary to be continuous at the edge of the cell is reasonable. However, in the case where there exists abundant extracellular matrix, the requirement that the impedance outside the cell be continuous at the cell boundary should be relaxed.

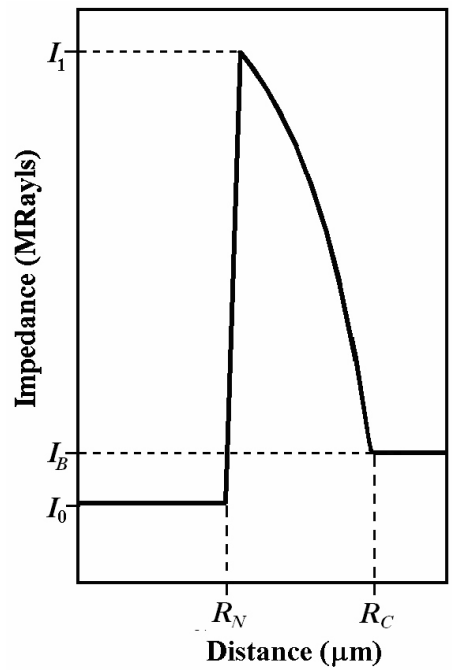

FIG. 3 1-D graphical representation of the new cell model with the nuclear impedance, I_0, the background impedance, I_B, the maximum cell cytoplasm impedance, I_1, the nuclear radius, R_N and the total cell radius, R_C.

Five variables were used to fit the new cell model to the normalized backscattered power spectra: (1) the nuclear impedance, I_0, (2) the maximum cell cytoplasm impedance, I_1, (3) the nuclear radius, R_N, (4) the total cell radius, R_C and (5) a gain factor. The curve describing the graded impedance was derived under the assumption that the number density of microtubules decreased with radial distance from the nucleus yielding

$$I \quad r \quad \frac{I_1 \quad I_B}{R_N^3 \quad R_C^3} r^3 \quad \frac{I_B R_N^3 \quad I_1 R_C^3}{R_N^3 \quad R_C^3} \tag{3}$$

where r is the radial distance with origin at the center of the nucleus. The impedance of the extracellular matrix (considered as a background material), I_B, was set to 1.5 MRayls. The choice of 1.5 MRayls was based on the appearance of the extracellular matrix as a fluid. Estimation of the ASD depends on the spatial variation of the impedance and not the absolute values of the impedance for each structure. The choice of the background impedance is somewhat arbitrary; however, the choice of background impedance determines the range of impedance values for the other structures. The gain factor was used to correct for any magnitude bias in the normalized power spectrum measured from the tumors and for any magnitude bias from the choice of background impedance. The gain factor simply added or subtracted a constant from the normalized power spectrum. The nuclear and maximum cell cytoplasm impedances were allowed to range between 1.30 and 1.70 MRayls or less than ± 15% of the background impedance. In the present study, estimates of ASD using the NCM were compared to the actual size of the nuclei of the cells in the tumors. The goodness of fit of the model to the measured data was assessed by the goodness-of-fit statistic, R^2.

B. Animal use

The experimental protocol was approved by IACUC (Institutional Animal Care and Use Committee, University of Illinois) and satisfied all campus and National Institutes of Health rules for the humane use of laboratory animals.

1. Mouse carcinomas

A mouse mammary tumor cell line (4T1 [CRL-2539]) was purchased from American Type Culture Collection (ATCC, Manassas, VA). This cell line was chosen because of its homogeneous cytologic characteristics and because the tumors are models for stage IV human breast cancer.[28-30] These cells were relatively uniform in morphology, oval to polygonal in shape with large prominent nuclei. Extracellular matrix was minimal to nonapparent. We used these cells as an *in vivo* model for uniform scattering statistics in tissues. The tumors model what might take place in an *in situ* form of breast carcinoma.

The 4T1 cells were cultured according to the process outlined in Oelze et al.[21] Cultured cells were injected into balb/c mice (Harlan, Indianapolis, IN). Mice were weighed and anesthetized with ketamine hydrochloride (87.0 mg/kg) and xylazine (13.0 mg/kg) administered intraperitoneally before injection with 4T1 cells. After the tumors reached 1.0 cm in diameter, mice were reanesthetized and humanely euthanized under anesthesia by cervical dislocation. The tumors were then ultrasonically imaged. Eight balb/c mice were used in this study. he nuclei of the cells were approximately 13 m in diameter with total cell sizes ranging between 25 to 30 m in diameter [21]

2. Mouse sarcomas

A mouse sarcoma tumor cell line (Englebreth-Holm-Swarm (EHS [CRL-2539]) was purchased from American Type Culture Collection (ATCC, Manassas, VA). This cell line was chosen because it produced abundant extracellular materials and basement membrane components (laminin, collagen IV, entactin, and heparan sulfate proteoglycan).[31, 21] Like the carcinoma cell line, the cells were relatively uniform in morphology, oval to polygonal in shape with large prominent nuclei. However, in the tumors, abundant extracellular matrix existed, leading to identifiable structural differences compared to the carcinoma tumors examined. We used these cells as an *in vivo* model for uniform scattering statistics (the cells were monomorphic) in tissues and to examine the role of extracellular matrix to ultrasonic scattering.

Cultured cells were injected into C57BL/6 mice (Harlan, Indianapolis, IN). Mice were weighed and anesthetized with ketamine hydrochloride (87.0 mg/kg) and xylazine (13.0 mg/kg) administered intraperitoneally before injection with EHS cells. After the tumors reached 1.0 cm in diameter, mice were reanesthetized and humanely euthanized under anesthesia by cervical dislocation. The tumors were then ultrasonically imaged. Eight C57BL/6 mice were used in this study. The cell sizes were approximately the same as the carcinomas with nuclei 13 m in diameter on average and total cell sizes ranging between 25 to 30 m in diameter. However, instead of having a uniform distribution of cells with minimal extracellular matrix like the carcinoma tumor, the sarcoma had abundant extracellular matrix surrounding groups of cells.

C. Ultrasound scanning procedures

A single-element weakly-focused transducer was used to scan the mice. The transducer had a measured center frequency of 20 MHz at the focus with a 70% -6 dB pulse/echo bandwidth (10-24 MHz). The aperture diameter of the 20 MHz transducer was 6 mm with a focus measured at 20 mm. An analysis bandwidth from 16 to 27 MHz was used to obtain scatterer property estimates. This analysis bandwidth was chosen because previous studies indicated

that statistically significant differences between the carcinoma and sarcoma backscattered power spectra existed above 16 MHz.[23]

The 20 MHz transducer was operated in pulse/echo mode through a Panametrics 5900 pulser/receiver. The signals were recorded and digitized on an oscilloscope (Lecroy 9354TM, Chestnut Ridge, NY) and downloaded to a PC computer for postprocessing. The 8-bit sampling rate of the received echo signals was 200 MHz. The transducer was moved laterally across the tumor by a micropositioning system with step size between each scan line of 50 m. The attenuation for both kinds of tumors was 0.4 dB MHz^{-1} cm^{-1} based on insertion loss measurements from sliced carcinoma and sarcoma tumor tissues. After scanning, tumors were excised, fixed in 10% neutral-buffered formalin, processed and embedded in paraffin, sectioned at 5 m, and stained with hematoxylin and eosin (H&E) for routine histologic evaluation by light microscopy.

The backscattered power spectra were measured for many ROIs within the tumors. The ROIs corresponded to 5 beamwidths laterally and 12 pulse lengths axially (gated with a Hanning window). The measured backscattered power spectrum for an ROI was found by averaging the backscattered power spectra measured from the echo signals corresponding spatially to the ROI. The measured backscattered power spectrum is given by[25]

$$W_{meas}(f) = \frac{1}{N} A(f, L) \sum_{n=1}^{N} \frac{\left| FT\{p_n(t)\} \right|^2}{W_{ref}(f)} \tag{4}$$

where $FT\{p_n(t)\}^2$ represents the Fourier transform of the gated rf signal of the nth scan line, N is the number of gated scan lines contained within a ROI, $A(f, L)$ is a frequency-dependent attenuation-compensation function and $W_{ref}(f)$ is the reference power spectrum.[33] The effects of the equipment on the power spectrum measurement were factored out by dividing by a reference spectrum.[2, 20, 25] The reference power spectrum was obtained by recording rf signals from reflections off a smooth planar surface of known reflectivity normal to the transducer beam axis. The planar reflector was translated from location at the front of the depth of field of the transducer to the back of the depth of field with a distance of 75 m (the wavelength at 20 MHz) between steps. At each point, the rf signal reflected from the smooth planar surface was recorded. The reference power spectrum for an ROI was calculated by averaging the squared magnitude of the Fourier transform of each reflected rf signal corresponding to the axial location of the ROI. The measured backscattered power spectrum was compensated for attenuation losses according to the frequency-dependent attenuation-compensation function, $A(f, L)$, derived for echo signals gated with Hanning windows.[33]

RESULTS

ASD images were constructed for the sarcomas and carcinomas using the three different models. Figure 4 shows ASD images of a carcinoma and sarcoma tumor using the three models. The tumors examined correspond to animal 2 for the carcinomas and animal 6 for the sarcomas. These animals were chosen because their images highlight the largest differences in average ASD estimates amongst the different models used. For example, the ASD image of the sarcoma using the FFSM (bottom panel, center image of figure 4) had an average ASD of 62.6 m compared to the average ASD value for all the animals examined using FFSM of 47.7 m. The large average ASD value for the particular tumor image in figure 4 reflects the large standard deviation of ASD estimates among the different animals when us-

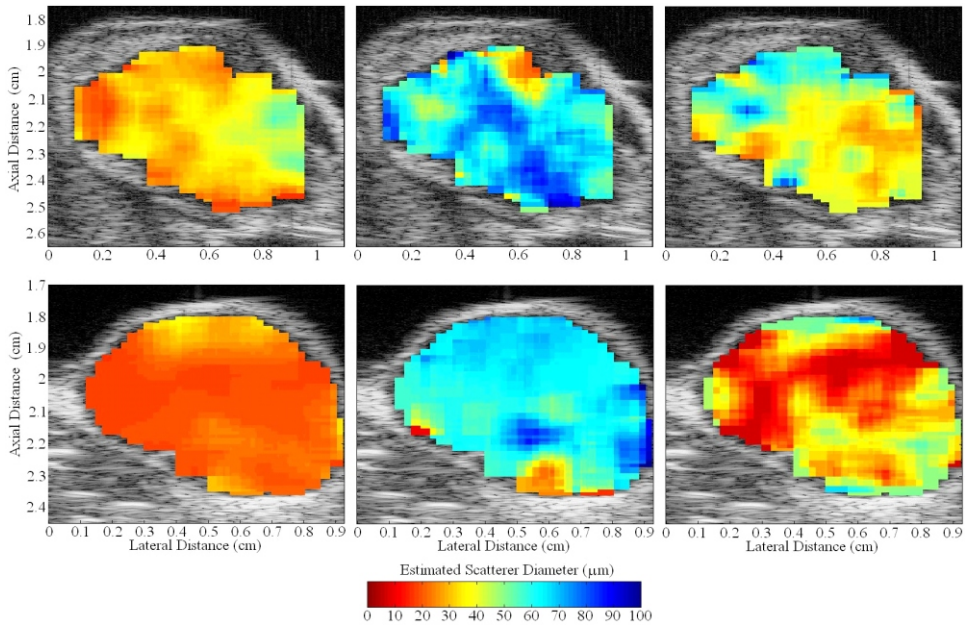

FIG. 4 ASD images of a mouse mammary carcinoma (top panel) and sarcoma (bottom panel) using the SGM (left images), the FFSM (middle images) and the NCM (right images).

ing the FFSM. The mean ASD estimates of the sarcoma using SGM and NCM were 18.8 m and 25.0 m, respectively, and almost three times smaller than the average obtained using the FFSM.

The ASD images of figure 4 were constructed by superimposing color-coded pixels on a conventional gray-scale B-mode image of the tumors. The size and location of the color-coded pixels corresponded to ROIs from which ASD estimates were obtained. A sliding Hanning window was used axially to range gate the signals corresponding to the ROIs with an overlap of 75%. Laterally, each ROI overlapped the next ROI by 75%. Therefore, each pixel represents the average from 16 ROIs. The color of the pixels corresponded to the ASD estimated for the ROI. The average number of independent ASD estimates for a single tumor was 30 for the carcinomas and 41 for the sarcomas. The average number of independent ASD estimates represents 1/16 of the average of the total number of estimates per tumor, i.e., the total number of ROIs.

The ASD estimates are listed in table 1 for the carcinomas and sarcomas. The largest overall differences between carcinomas and sarcomas were observed when the SGM or NCM were used to fit the measured data. The sizes of the standard error of the mean (SEM) values were small in all cases (< 1.0 for the SGM, < 2.5 for the NCM and FFSM) because each tumor contained more than 30 independent estimates. The number of independent samples for each solid tumor is important because the more independent estimates that existed for a tumor, the smaller the SEM. Because the SEM was small, the ASD for a tumor was a good representation of the tumor as a whole.

The ASD estimates from each set of the eight animals were then averaged to get an ASD for each group (carcinomas and sarcomas). Table 2 lists the mean ASDs for the carcinomas and sarcomas versus each model type along with the standard deviation. The standard deviation represents the variation from animal to animal within a group. The goodness-of-fit statistic listed in table 2 reveals that the SGM had the worst fit to the data followed by the FFSM. However, it is important to note that all of the models performed poorly as revealed by the

TABLE 1. Estimated ASDs m for each animal and the corresponding standard error of the mean value.

	Carcinoma animal number							
Model	**1**	**2**	**3**	**4**	**5**	**6**	**7**	**8**
SGM	32.0; 0.93	32.6; 0.98	32.0; 0.95	31.0; 0.85	23.9; 0.69	28.2; 0.69	33.1; 0.96	29.7; 0.88
FFSM	48.6; 2.28	63.0; 2.52	42.2; 2.17	51.4; 2.10	37.0; 2.11	48.6; 2.00	46.8; 2.40	40.4; 2.73
NCM	42.6; 2.66	41.6; 1.94	40.4; 2.45	41.4; 2.17	38.6; 3.52	40.8; 2.07	43.1; 2.56	41.0; 3.15
	Sarcoma animal number							
Model	**1**	**2**	**3**	**4**	**5**	**6**	**7**	**8**
SGM	28.2; 0.55	30.7; 0.52	28.6; 0.49	25.0; 0.36	20.6; 0.44	18.8; 0.48	22.2; 0.48	26.0; 0.50
FFSM	40.8; 1.95	43.6; 3.00	46.5; 3.27	42.0; 2.01	51.2; 1.74	62.6; 1.65	45.8; 2.11	48.0; 2.51
NCM	36.8; 2.04	38.5; 1.53	44.0; 2.85	35.5; 1.90	28.3; 1.93	25.0; 2.30	35.2; 2.18	32.0; 1.95

TABLE 2. Mean of the ASDs (m) for eight tumors, their corresponding standard deviations, the average goodness of fit, R^2 and the system (cell or nucleus) that the ASD estimate is hypothesized to describe.

	Carcinomas		**Sarcomas**		
	<D> ± S.D.	**$<R^2>$**	**<D> ± S.D.**	**$<R^2>$**	
SGM	30.3 ± 3.06	0.12	25.2 ± 4.01	0.24	Cell 25-30 m
FFSM	47.3 ± 7.99	0.26	47.7 ± 7.01	0.36	Nucleus 13 m
NCM	41.2 ± 1.39	0.28	34.4 ± 5.95	0.37	Nucleus 13 m

goodness-of-fit statistic. The largest R^2 value occurred with the NCM and the sarcomas, i.e. $R^2 = 0.37$. For comparison with histological analysis, the actual size of the object hypothesized to be estimated by each model is listed. For the NCM, average estimates of nuclear impedance, I_0, and the maximum cell cytoplasm impedance, I_1, were 1.60 MRayls and 1.57 MRayls, respectively, for both kinds of tumors.

Analysis of the variance (ANOVA) was conducted on ASD estimates from the rows of table 1 for each model. statistically significant differences were observed between the carcinomas and sarcomas when using the SGM and NCM ($P < 0.05$). statistically significant differences between the carcinomas and sarcomas were not observed when using the FFSM ($P \sim 0.91$).

DISCUSSION AND CONCLUSIONS

Two kinds of tumors, mammary carcinoma and mammary sarcoma, were examined using ultrasound, and their scatterer properties were estimated. The morphology of the tumors was previously observed from optical photomicrographs to be distinctly different.[23] The carcinomas contained a uniform distribution of cells with minimal extracellular matrix. The sarcomas contained groups of cells consisting of one to a dozen cells surrounded by abun-

dant extracellular matrix. However, previous ultrasound spectral analysis using ASD estimates did not detect these differences. F-tests of the normalized backscattered power spectra from the two kinds of tumors revealed statistically-significant differences existed when the frequency of ultrasound was above 16 MHz.

Three models for the spatial distribution of acoustic impedance from scattering tissues were proposed. From these three models, the backscattered power spectra were calculated and used to extract ASD estimates from two kinds of solid tumors in mice using an analysis bandwidth from 16 to 27 MHz. The SGM is a model that has been used in various spectral imaging studies. The ASD estimates from the SGM model were hypothesized to represent the total cell size. The FFSM was used to model scattering from cell nuclei as fluid-filled spheres in a constant background that corresponded to the cell cytoplasm and extracellular matrix. The ASD estimates from the FFSM model were hypothesized to represent the average nuclear diameter. The NCM was used to model scattering from the cell composed of both a nucleus and cytoskeleton. Comparison of the ASD estimates with the sizes of the objects that were hypothesized to be modeled (table 2) indicates that the SGM model came closest to representing the hypothesized scatterer. The FFSM and NCM models yielded ASD estimates that were three to four times larger than the objects they were hypothesized to represent. Therefore, the FFSM and NCM did not appear to accurately represent the microstructures hypothesized as responsible for scattering from optical photomicrographs of the tissues. Comparison of the ASD estimates with underlying microstructure suggests that cells (as opposed to the nuclei of cells) or structures in the size range of cells are a dominant source of scattering from these tumors. For example, the ASD estimates from the FFSM would suggest modeling the total cell as a fluid-filled sphere and not just considering the nucleus as important to scattering.

Scatterer property estimates using the NCM and SGM did reveal statistically significant differences between the two kinds of tumors. The estimated ASD (modeled as the cell nuclei) using the NCM were 41.2 ± 1.39 m and 34.4 ± 5.95 m for the carcinomas and sarcomas, respectively. The estimated ASD using the SGM were 30.3 ± 3.06 m and 25.2 ± 4.01 m for the carcinomas and sarcomas, respectively. Scatterer property estimates using the FFSM did not reveal statistically significant differences between the two kinds of tumors. Furthermore, the estimated ASD (modeled as the cell nuclei) was approximately 48 m using the FFSM for both kinds of tumors compared to the actual nuclear diameters of approximately 13 m.[21]

The goodness of fit as determined by the R^2 statistic revealed that none of the models explained the measured power spectra very well. The average R^2 statistic was less than 0.37 for each model used. Even though the models did not produce good fits to the data as determined by the R^2 statistic, statistically significant differences between the carcinomas and sarcomas were revealed through ASD estimates using the SGM and NCM. Surprisingly, ASD estimates using the FFSM did not reveal statistically significant differences even though the R^2 statistic indicated better fits to the data than the SGM. While all models poorly accounted for the data, the SGM and NCM appeared to be sensitive to portions of the backscattered power spectra that enabled differences between the carcinomas and sarcomas to be observed. The FFSM did not appear to be sensitive to portions of the backscattered power spectra that could lead to the observation of statistically significant differences.

The SGM and NCM models were able to detect statistically significant differences between the two kinds of tumors. While statistically significant differences were observed, examination of table 2 suggests that the estimates did not faithfully represent the actual microstructural differences as observed from photomicrographs of the tumors.[23] To more faithfully represent the underlying sources of scattering, better acoustic impedance values of cells and extracellular matrix must be determined and corresponding models constructed. Better acoustic impedance values for the microstructures and corresponding models will in-

crease the potential for discovering statistically-significant differences between different kinds of tumors using spectral techniques.

Estimates of nuclear impedance and cytoplasm impedance from the NCM revealed a larger impedance value for the nucleus (1.60 MRayls versus 1.57 MRayls). An examination of mechanical properties of cellular components from other studies reveals a larger range of values for the different components. For example, acoustical microscope measurements of sound speed of the nucleus of HaCaT cells revealed a range of estimates from 1,500 m/s to 1,650 m/s.[34] Other researchers have estimated sound speeds for DNA and cell nuclei ranging from 1,700 to 1,800 m/s.[35-37] The values for the different cellular components depend on the method in which the cellular components were isolated and the measurement technique used to extract the mechanical properties. No standard method exists to extract the mechanical properties of cellular components due to various methods of isolation and measurement techniques. If a better scattering model of the cell could be constructed, then it might be possible to extract mechanical properties of cells by fitting the model to the backscattered power spectrum without isolating individual cell components. The goodness-of-fit parameters obtained with the present NCM model do not suggest the present model is adequate for extracting reliable estimates of impedance values for cell component structures.

Analysis of improved models can also help suggest appropriate frequency ranges to use in ultrasonic interrogation of tumors. Previous studies using the SGM over the frequency range of 10 to 27 MHz yielded scatterer property estimates that did not reveal statistically-significant differences in the two kinds of tumors examined.[23] However, statistically significant differences were observed when using the SGM over the frequency range of 16 to 27 MHz. The choice of an appropriate ultrasound frequency range was vital for finding statistically significant differences between the two tumors.

Another important consideration to providing statistically significant differences between different kinds of tumors is the large number of independent estimates obtained for any one tumor examined. The large number of independent estimates led to smaller SEM values. By averaging many independent estimates, a large variance in one estimate (from the mean) will have little effect on the average. For this reason, the SEM is a more suitable variable for determining how well the mean estimate value describes a particular tumor. The more independent estimates from a tumor there are, the better the overall characterization of the tumor. Because there were more than 30 independent estimates per tumor, statistically-significant differences between the two kinds of tumors could be determined from the ASDs from the tumors.

In the cases examined in this study, the individual estimate variance was not the limiting factor in differentiating one tumor type from another. However, estimate bias may play a role in determining statistically significant differences. The estimate bias can be introduced by several factors including the amount and type of attenuation compensation used, calibration and measurement technique and model used. Examination of the models used in this study revealed that each model yielded different mean estimates for each tumor type. Further, some models were able to produce estimates that allowed distinguishing between different kinds of tumors while others (the FFSM) were unable to produce these statistically-significant differences. Improving attenuation compensation, measurement techniques and models can improve the ability to distinguish between different kinds of tumors provided enough independent estimates can be obtained. For small tumors with small numbers of independent estimates or for mapping out tumor margins using scatterer property estimates, the spectral techniques may be limited by estimate variance.

No direct study of the correlation of the variance in ASD estimates from the scatterers and the variance in actual sizes of the hypothesized scattering sources (e.g., the cells or nuclei) was conducted. Examination of the ASD images of figure 4 indicates significant variance in

ASD estimates throughout some of the tumors. Whether this variance is due to experimental uncertainty, modeling insufficiencies or underlying biological variance has not been determined. Further study needs to be conducted to determine the actual sources responsible for scattering and to compare the biological variance of the sources of scattering and their relation to the variance of scatterer property estimates.

ACKNOWLEDGEMENTS

The author wishes to recognize the pioneering work of Dr. Frederic Lizzi that has led to the present study. This work was supported by NIH F32 CA96419 to MLO and by start-up funds provided by the Department of Electrical and Computer Engineering at the University of Illinois at Urbana-Champaign.

REFERENCES

1. Nicholas D. Evaluation of backscattering coefficients for excised human tissues: results interpretation, and associated measurements, *Ultrasound Med Biol 8*, 17-28 (1982).

2. Lizzi FL, Greenebaum M, Feleppa EJ, Elbaum M, Coleman DJ. Theoretical framework for spectrum analysis in ultrasonic tissue characterization, *J Acoust Soc Am 73*, 1366-1373 (1983).

3. Miller JG, Perez JE, Mottley JG, et al. Myocardial tissue characterization: an approach based on quantitative backscatter and attenuation, in *Ultrasonics Symp Proc* 2, 782-793 (1983).

4. D'Astous FT, Foster FS. Frequency dependence of ultrasound attenuation and backscatter in breast tissue,. *Ultrasound Med Biol 12*, 795-808 (1986).

5. Nassiri DK, Hill CR. The use of angular scattering measurements to estimate structural parameters of human and animal tissues, *J Acoust Soc Am 79*, 2048-2054 (1986).

6. Sigelmann RA, Reid JM. Analysis and measurement of ultrasound backscattering from an ensemble of scatterers excited by sine-wave bursts, *J Acoust Soc Am 53*, 1351–1355 (1973).

7. O'Donnell M, Miller JG. Quantitative broadband ultrasonic backscatter: An approach to nondestructive evaluation in acoustically inhomogeneous materials, *J Appl Phys 52*, 1056–1065 (1981).

8. Coleman DJ and FL Lizzi. Computerized ultrasonic tissue characterization of ocular tumors*, Amer J Ophthal 96*, 165-175 (1983).

9. Coleman DJ, Rondeau MJ, Silverman RH, Lizzi FL. Computerized ultrasonic biometry and imaging of intraocular tumors for monitoring of therapy,. *Trans Am Opthalmol Soc 85,* 48-81 (1987).

10. Coleman DJ, Silverman RH, Rondeau MJ, et al. Correlations of acoustic tissue typing of malignant-melanoma and histopathologic features as a predictor of death,. *Amer J Ophthal 110*, 380-388 (1990).

11. Coleman DJ, Silverman RH, Rondeau MJ, et al. Ultrasonic tissue characterization of uveal melanoma and prediction of patient survival after enucleation and brachytherapy,. *Amer J Ophthal 112*, 682-688 (1991).

12. Coleman DJ, RH Silverman, MJ Rondeau, et al. Noninvasive in vivo detection of prognostic indicators for high-risk uveal melanoma: ultrasound parameter imaging,. *Ophthalmology 111*, 558-564 (2004).

13. Feleppa EJ, Lizzi FL, Coleman DJ, Yaremko MM. Diagnostic spectrum analysis in ophthalmology: a physical perspective, *Ultrasound Med Biol 12*, 623-631 (1986).

14. Feleppa EJ, Kalisz A, Sokil-Melgar JB, et al. Typing of prostate tissue by ultrasonic spectrum analysis, *IEEE Trans Ultrason Ferro Freq Cont 43*, 609-619 (1996).

15. Feleppa EJ, Liu T, Kalisz A, et al. Ultrasonic spectral-parameter imaging of the prostate, *Int J Imaging Syst Technol 8*, 11-25 (1997).

16. Lizzi FL, Astor M, Liu T, et al. Ultrasonic spectrum analysis for tissue assays and therapy evaluation, *Int J Imaging Syst Technol 8*, 3-10 (1997).

17. Silverman RH, Folberg R, Boldt HC, et al. Correlation of ultrasound parameter imaging with microcirculatory patterns in uveal melanomas, *Ultrasound Med Biol 23*, 573-581 (1997).

18. Lizzi FL, Ostromogilsky M, Feleppa EJ, Rorke MC, Yaremko MM. Relationship Of ultrasonic spectral parameters to features of tissue microstructure, *IEEE Trans Ultrason Ferro Freq Cont 34*, 319-329 (1987).

19. Landini L, Sarnelli R, Salvadori M, Squartini F. Orientation and frequency-dependence of backscatter coefficient in normal and pathological breast tissues,. *Ultrasound Med Biol 13*, 77-83 (1987).

20. Oelze ML, Zachary JF, O'Brien, Jr. WD. Characterization of tissue microstructure using ultrasonic backscatter: theory and technique optimization using a Gaussian form factor, *J Acoust Soc Am 112,* 1202-1211 (2002).

21. Oelze ML, Zachary JF, O'Brien, Jr. WD. Differentiation and characterization of mammary fibroadenomas and 4T1 Carcinomas using ultrasound parametric imaging, *IEEE Trans Med Imag 23*, 764-771 (2004).

22. Oelze ML, O'Brien, Jr. WD, Zachary JF. High frequency quantitative imaging of solid tumors in mice, in *Proc 28th Int Acoust Imag Symp*, San Diego, CA (2005) (in press).

23. Oelze ML, Zachary JF. Examination of cancer in mouse models using quantitative ultrasound, *Ultrasound Med Biol* (2006) (in press).

24. Morse PM, Ingard KU. *Theoretical Acoustics.* (New York, McGraw-Hill, 1968).

25. Insana MF, Hall TJ. Parametric ultrasound imaging from backscatter coefficient measurements - image-formation and interpretation, *Ultrasonic Imaging 12*, 245-267 (1990).

26. Mamou J, Oelze ML, O'Brien, Jr. WD, Zachary JF. Identifying ultrasonic scattering sites from 3D impedance maps, *J Acoust Soc Am 117*, 413-423 (2005).

27. Anderson VC. Sound scattering from a fluid sphere, *J Acoust Soc Am 22*, 426-431 (1950).

28. Aslakson CJ, Miller FR. Selective events in the metastatic process defined by analysis of the sequential dissemination of subpopulations of a mouse mammary tumor, *Cancer Res 52*, 1399-1405 (1992).

29. Pulaski BA, Ostrand-Rosenberg S. Reduction of established spontaneous mammary carcinoma metastases following immunotherapy with major histocompatibility complex class II and B7.1 cell-based tumor vaccines, *Cancer Res 58*, 1486-1493 (1998).

30. Pulaski BA, Terman DS, Kahn S, Muller E, Ostrand-Rosenberg S. Cooperativity of *staphylococcal aureus* enterotoxin B superantigen, major histocompatibility complex class H, and CD80 for immunotherapy of advanced spontaneous metastases in a clinically relevant postoperative mouse breast cancer model, *Cancer Res 60*, 2710-2715 (2000).

31. Kleinman HK, McGarvey ML, Hassell JR, et al. Basement membrane complexes with biological activity. *Biochemistry 25*, 312-318 (1986).

32. Timpl R , Rohde H, Robey PG, et al. Laminin – a glycoprotein from basement membranes. *J Biol Chem 254*, 9933-9937 (1979).

33. Oelze ML, O'Brien, Jr. WD. Frequency-dependent attenuation-compensation functions for ultrasonic signals backscattered from random media, *J Acous Soc Am 111*, 2308-2319 (2002).

34. Kundu T, Blasé, C, Bereiter-Hahn J. Determination of cell properties from single and multi-layered cell models, in *Proc SPIE 5768*, 44-54 (2005).

35. Maret G, Oldenbourg R, Winterling G, Dransfeld K, Rupprecht A. Velocity of high frequency sound waves in oriented DNA fibres and films determined by Brillouin scattering, *Colloid Poly Sci 257*, 1017-1020 (1979).

36. Hakim MB, Lindsay SM, Powell J. The speed of sound in DNA *Biopolymers 23,* 1185-1192 (1984).

37. Bishop TC, Zhmudsky OO. Mechanical model of the nucleosome and chromatin. *J Biomed Struct Dyn 19*, 878-888 (2002).